Proceedings of the
IASTED International
Conference

Robotics & Manufacturing

Cancun, Mexico
May 21-24, 2001

Editor: M.H. Hamza

A Publication of The International Association of Science and Technology for Development - IASTED

ISBN: 0-88986-281-8
ISSN: 1027-264X

IASTED/ACTA Press

Anaheim * Calgary * Zurich

Proceedings of the
IASTED International
Conference

Robotics & Manufacturing

Cancun, Mexico
May 21-24, 2001

Editor: M.H. Hamza

A Publication of The International
Association of Science and Technology
for Development - IASTED

ISBN: 0-88986-281-8
ISSN: 1027-264X

IASTED/ACTA Press

Anaheim * Calgary * Zurich

Table of Contents

Manufacturing Systems and New Technologies

Sensing and Data Fusion

Vision, Virtual Environments, and Simulation Models

Papers from Other IASTED Conferences

Proceedings of the IASTED International Conference
ROBOTICS AND MANUFACTURING
May 21-24, 2001, Cancun, Mexico

A NEW ROBOT DESIGN TO PASSIVELY DAMP FLEXIBLE ROBOTIC ARMS

Louis J. Everett
Mechanical and Industrial Engineering
University of Texas El Paso
USA

Marc Compere
Mechanical Engineering Department
University of Texas at Austin
USA

ABSTRACT

This paper presents a hardware configuration for a long reach robotic arm in which passive dampers eliminate unwanted oscillation. This paper derives and reduces the equations of motion for the proposed configuration; then develops a "realistic" design. Using a single degree of freedom approximation, the paper presents and experimentally verifies equations for the dominant natural frequency and damping ratio. The paper demonstrates that the equations are good predictors of dynamic response for a large set of robots. The design is verified via experiment.

KEY WORDS: Robot Design, Modeling, Space Robotics

1. INTRODUCTION

Long reach robot arms are being designed and implemented in space applications as well as the Department of Energy's Environmental Waste Management projects. Most of the robots currently being produced or proposed, are single cantilever beam devices. There are at least two problems with this design. First, long reach robot arms are inherently prone to vibration. Second, during vibration the robot tip not only translates, but also rotates. This second problem can be especially critical if the robot needs to hold a tool against a stationary object.

The two broadest categories of methods used to combat the vibration problem are active control and passive energy dissipation methods. The actively controlled methods [1],[2] have been proven effective in damping oscillations, however are often complex and are more prone to sensor, actuator, or computation failure than passive methods.
Passively damping vibration has several advantages over actively controlled systems. First, as mentioned previously, it reduces the robot's complexity and improves reliability by reducing the possibility of computer, sensor, or actuator failure. Second, it eliminates power consumption from sensing, actuation, or on-line computing. Finally, if the undamped system is stable adding passive dampers cannot cause instability. A major problem with passive damping is designing a system that has a significant damping factor. For example, one passive scheme [3] uses a coating to dissipate vibrational energy. This method is reliable, simple, and works well for higher frequencies. However, it does not provide as high a damping ratio as many actively controlled schemes.

Other "active" methods include inverse dynamics [4] and input shaping techniques [5]. These methods essentially work to avoid introducing vibrational energy, so it is unclear whether they should be called damping methods in a strict sense.

This paper presents another method for passively damping oscillation in robot arms that rivals the damping produced with active methods. It is based on a parallel beam design constructed to produce points in the structure that have large relative motions. One connects passive dampers between these points thereby producing significant damping. The analysis presented here demonstrates how to design a system that effectively and passively controls vibration. This is in contrast to a post-design solution for vibration reduction using active methods. A reduced model of the system provides design tools, such as equations and graphs, from which a prospective designer can predict the dynamic response of the robot.

2. THE NEW CONCEPT

The proposed configuration replaces the single flexible link with two parallel flexible links. This design provides the opportunity for passive dampers to utilize the relative velocities between the beams to dissipate energy associated with tip vibration. Figure 1 shows a parallel, flexible beam configuration in deflection. Similar to a four-bar linkage, the distance between points one and four changes during tip deflection. Likewise, the distance between two and three also changes.

The first difference between traditional robot arm designs and the new concept is the amount of tip rotation. For a single-beam configuration, the end-mass rotation is dependent on beam deflection. But if the following four

conditions are met, the new configuration, has negligible tip rotation:

- there is negligible axial deflection in the side beams
- there is no buckling
- there is negligible play in the joints and hinges
- the distance between beam tips remains constant during deflection

One benefit of the negligible end-mass rotation is that it produces a 'stable platform' at the tip. This is potentially useful during maneuvers where it is important to maintain a constant tip orientation. This would occur for example, when the robot is grinding a surface or pressing a sensor against a surface. A second benefit of negligible tip rotation is that the motion of the manipulator is independent of the end-mass rotational inertia.

A second difference between the new design and conventional mechanisms is that the passive dampers can be completely contained within the robot structure.

The proposed manipulator design is similar to a truss. The differences between the configuration in this paper and existing truss designs include the following:

- Truss designs typically have large widths whereas the proposed design is much narrower. For example the width to length ratios used in the experiments in this paper are close to those of NASA's Space Shuttle manipulator arm.
- Truss designs typically have several "cross members" along the length of the mechanism. These cross members stiffen the truss but also add weight. Our design does not use "cross members" as a means to increase rigidity. They are used only as a lightweight means to synchronize the motion of the two deflecting beams. Because the proposed design has fewer cross members, it weighs less.

3. MODELING

A flexible cantilever beam can be approximated by a finite number of rigid links coupled with torsional springs. The torsional spring constants were derived such that the deflections along the approximated beam were identical to a static cantilever beam. Applying this approach to the proposed configuration, the two flexible beams are modeled by pairs of rigid links. Each link has crossbars at each joint. This is shown in Figure 2.

Multi Degree of Freedom Models

Using many rigid links to approximate the flexible beams increases model fidelity in two ways. First, it increases the model's ability to approximate the cubic deflection curve of a static cantilever beam in deflection. Second, it increases the number of natural frequencies the model can predict. However, as the number of rigid links increases, the non-linear equations of motion become complex and using them for physical insight into the system behavior is too difficult. We used the multi degree-of-freedom (DOF) models for verifying our design derived from a single DOF model. We did this in two steps. First, we matched the multi DOF model to experimental data verifying the mathematics. Second, because the multi DOF model shows the contribution of higher-order dynamics, we used it to test the design rules extracted from the single DOF model.

Single Degree of Freedom Model

The simplest flexible parallel beam approximation is a four-bar linkage. After linearization, the equation of motion (EOM) for the single DOF model is simple enough to provide physical insight and is useful for developing equations to predict dynamic response.

Our philosophy in using this one degree of freedom model is to utilize the simplest model that sufficiently describes the phenomenon being studied. The question of course is whether or not the simple model describes the phenomena we want to explain. To answer the question it is important to identify what phenomena are important. For example, a lumped mass model of a flexible manipulator with input torque at the base is minimum phase but a continuum model is not. This can be significant if we are attempting to control the manipulator using information about the end effector position. What is more interesting however is understanding what physical characteristics affect the amount of damping we can achieve. In our opinion, our experiments (which we show later) establish the model's validity since the damping we measured matched the simple model quite well.

After using Lagrange's method to derive a single, second-order differential equation, linearization techniques were used to simplify the EOM as shown in Equation (1). Equating the coefficients to the standard second order system, gives expressions for the dominant natural frequency and damping ratio in terms of robot parameters.

$$\ddot{\Theta}+\left(\frac{C_{total}}{(1+A^2)M_{eq}}\right)\dot{\Theta}+\left(\frac{6EI}{L_{total}^3 M_{eq}}\right)\Theta=0 \qquad (1)$$

The variable Θ is the deflection of the beam from equilibrium. The resulting expressions for equivalent frequency and damping ratio are given in Equations (2) and (3).

$$\omega_n=\sqrt{\frac{6EI}{L_{total}^3 M_{eq}}} \qquad (2)$$

$$\zeta=\frac{C_{total}}{2(1+A^2)M_{eq}\omega_n} \qquad (3)$$

The term "A" in Equation (3) is the "aspect ratio" defined as Ltotal/d. Ltotal is the total flexible beam length and Ctotal is the summation of all damper coefficients in the system. Meq is a weighted sum of all masses in the system and contains the link masses, crossbeam masses, and the end-mass. Equation (4) defines Meq and it accounts for the various mass' distribution along the length of the robot.

$$M_{eq} = aM_{rigid-link} + bM_{crossbeams} + cM_{end-mass} \quad (4)$$

The process of determining a, b and c follows. First, rearrange the terms to form Equation (5):

$$M_{eq} = \frac{6EI}{L_{tot}^3 \omega_n^2} \quad (5)$$

Next, we simulated the double-stage model three times using various values (see the Model Validation section). For each simulation, we applied small perturbations in each mass. As a result, we constructed the following expression for equivalent mass:

$$\begin{bmatrix} M_{r.l.-1} & M_{cross-1} & M_{end-1} \\ M_{r.l.-2} & M_{cross-2} & M_{end-2} \\ M_{r.l.-3} & M_{cross-3} & M_{end-3} \end{bmatrix} \begin{bmatrix} a \\ b \\ c \end{bmatrix} = \begin{bmatrix} M_{eq-1} \\ M_{eq-2} \\ M_{eq-3} \end{bmatrix} \quad (6)$$

After each of the three simulations, the natural frequency was recorded and used to calculate Meq with Equation (5). The coefficients a, b, and c were then determined using Equation (6). The final step was to normalize the coefficients in Equations (4) and (6) such that the $M_{end-mass}$ coefficient was 1.0.

We used a similar procedure to calculate Meq for higher DOF rigid link models. Because the linearization procedure depends on numeric simulation data, small variations in the magnitude of Meq can arise as a result of both round-off error and the point about which it is linearized.

The final expressions used for Meq with the double and triple stage models were:

$$M_{eq-double-stage} = (1.0)M_{rigid-link} + (1.1)M_{crossbeams} + (1.0)M_{end-mass} \quad (7)$$

$$M_{eq-triple-stage} = (1.43)M_{rigid-link} + (0.983)M_{crossbeams} + (1.0)M_{end-mass} \quad (8)$$

4. EXPERIMENTAL SETUP

The experimental apparatus consists of two flexible aluminum beams rigidly attached to a base as shown in Figure 3. A calibrated DC-response accelerometer collected tip acceleration measurements. During large end-mass experiments, an air bearing supported the tip to prevent torsional deflection in the beams. The hardware was carefully adjusted to (1) eliminate free play in the joints, and (2) to make sure the long beams were parallel.

5. MODEL VALIDATION & PARAMETER IDENTIFICATION

To validate the mathematical model, the non-linear differential equations for the double-stage model were numerically integrated. For initial conditions, the model's first mode shape and initial tip deflection were matched to those of the experimental setup.

We measured model parameters from the experimental apparatus and made two minor adjustments. First, we adjusted the beam thickness by less than 1% of its measured value to make the natural frequency match the experiment. Second, we adjusted the end mass magnitude less than 4% to make the "large end load" frequency match. Figure 4 shows a typical comparison between computed and measured values.

To determine the damping coefficients, we installed the dampers on a simple spring mass system hanging vertically. We measured the mass and spring rate. An accelerometer measured the vibration of the damped system. Using a log-decrement calculation, we determined the damping coefficients. Inserting these values without any modification directly into the double-stage model and simulating the response allowed us to compare the damped model to the damped experimental apparatus. Figure 5 shows the typical agreement in the damped responses.

The experimental data reveal that there are components of both Coulombic friction and structural damping present. The near-linear decay during the initial portion of the undamped experimental responses shows that, within that range, Coulombic friction is the primary source of energy dissipation. The gradual curve on the experimental plots near the steady state region is similar to an exponential decay. This indicates the dominant source of damping at this point is primarily from structural damping. One can ignore these effects for two reasons. First, the time scale on the undamped plots is 4 - 5 times greater than those on the damped plots. This indicates the intrinsic damping in the experimental rig is negligible compare to what the damper provides. Second, the damped response graphs show good agreement between the predicted decay rate and the experimental data.

Considering the size of the two model adjustments and the level of agreement in the plots, we concluded that the double-stage model is a good predictor of the experimental response.

6. EFFECT OF A REALISTICALLY SIZED MANIPULATOR

One aim of this study is to provide tools for designing similarly configured flexible robots. To extend findings from small-scale models to full-size prototypes, we want to understand the effect of scale. Once this effect is understood, the equations will be presented as predictors of dominant natural frequency and damping ratio for any similar flexible robot.

The scale concept we plan to use is to allow all length dimensions to change by a scale factor S. All other physical quantities remain the same. For example the beam length and width might double, but the density and Young's modulus of the material remains constant. During the first investigation, several parameters will change in such a way that the equations predict the same response. The second demonstration will predict natural frequency and damping ratio of a full-sized robot made with the same material as the experimental model. The full-sized robot will use "realistic" parameters.

Selective Scalability

Table 1 shows four sets of parameters that represent selective scaling from the nominal, or experimental, setup. The four configurations are different in ways such that Equations (2) and (3) predict the same dynamic response. Figure 6 is a graph of the simulation of the double-stage model's normalized tip deflection using the four configurations in Table 1. The simulation output is presented in a dimensionless form by dividing the actual tip deflection by the initial deflection.

Table 1. Selectively Scaled Parameters

	M_{eq}	EI	L_{tot}^3	C_{tot}	L_{tot}	A
1	0.0912	0.7154	0.7217	128	0.897	16.0
2	0.0912	7.154	7.217	592	1.93	34.5
3	0.912	0.7154	0.07217	280	0.416	7.43
4	0.912	7.154	0.7217	1280	0.897	16.0
	Independently Varied Quantities				Result	

The simulations show that the response of the various systems is essentially identical. This was predicted by the simple equations. From these results we conclude that Equations (2) and (3) are selectively scaleable. This means (at least within the parameter ranges simulated) the equations are good predictors of both the dominant natural frequency and damping ratio for a similarly configured flexible robot.

Error Summary for the Prediction Equations

Using the prediction equations, (3) and (4), with the parameters in Table 1, the calculated frequency and damping ratios are shown in Table 2 along with the values from the double-stage model simulations. Note that configurations 1 & 2 have small payloads while configurations 3 & 4 have large payloads. The small errors shown in Table 2 verify that the values predicted by the simplified equations match the values determined using a more complex model. This gives us evidence that the simple equations capture the important behavior of the system.

Table 2. Prediction Equation Error Summary

	Calc ω_n	Calc ζ	Simu ω_n	Simu ζ	% Δ in ω_n	% Δ in ζ
1	8.076	0.338	8.225	0.352	1.84 %	4.14 %
2	8.076	0.337	8.240	0.3514	2.03%	4.15 %
3	8.076	0.338	8.231	0.3510	1.92 %	3.85 %
4	8.076	0.338	8.225	0.352	1.84 %	4.14 %
	From Eqs (2) & (3)		From double-stage simulations			

Example Design Scenario

For predicting the dynamic response of an industrial long-reach robot, we present an example to show the design feasibility as well as the procedure used to predict natural frequency and damping characteristics. The proposed robot will be scaled-up from the experimental apparatus by a factor of 10. Introducing a scale factor, S=10, the following equation development demonstrates the repercussions of a geometric increase in all lengths. The goals are: First, predict the natural frequency of the scaled robot. Second, to find the linear damping coefficient, C_{tot}, that will yield a desired damping ratio. Third, to confirm that the required individual "full sized" damper C is feasible.

Since $I_{nominal} = \frac{1}{12} bh^3$, the scaled area moment of inertia is:

$$I_{scaled} = \frac{1}{12}(Sb)(Sh)^3 = \frac{1}{12} bh^3 S^4 = I_{nominal} S^4$$

Because each mass term in Equation (4) can be represented as, $M_{nominal,i} = \rho_i V_{nominal,i}$, and the resulting scaled volumes are $V_{scaled,i} = (S^3) V_{nominal,i}$ then the scaled equivalent mass can be represented as:

$$M_{eq,scaled} = (S^3) M_{eq,nominal}$$

Substituting $L_{total,scaled} = (S)L_{total,nominal}$ along with I_{scaled} and $M_{eq,scaled}$, gives Equation (9) showing the scaled natural frequency.

$$\omega_{n,scaled} = \sqrt{\frac{6EI_{scaled}}{(L_{total,scaled})^3 (M_{eq,scaled})}}$$

$$= \sqrt{\frac{6EI_{nominal}}{(L_{total,nominal})^3 M_{eq,nominal}} \left(\frac{1}{S^2}\right)} \qquad (9)$$

$$= \frac{\omega_{n,nominal}}{S}$$

This equation shows that the full size robot will have a lower natural frequency compared to the experiment.

One can use the same procedure to show how both the aspect ratio (defined as $A_{onminal} = L_{total} / d$) and the damping ratio are affected by a scaling factor.

$$A_{scaled} = \frac{SL_{total}}{Sd} = A_{nominal}$$

Because a scale factor for C_{total} would require knowledge about the particular geometry and configuration of the damper, there is no general way to scale the damping coefficient. Rather, the parameter C_{total} is held constant while developing the scaled damping ratio. Then as part of the design procedure, C_{total} can be whatever is necessary to produce the desired scaled damping ratio.

Substituting only $M_{eq,scaled}$ and Equation (9) into (3) yields

$$\zeta_{scaled} = \frac{C_{total}}{2(1+A^2)(S^3 M_{eq,nominal})} \left(\frac{S}{\omega_{n,nominal}}\right) \qquad (10)$$

$$= \frac{C_{total}}{(2(1+A^2)M_{eq,nominal}\ \omega_n)S^2} = \frac{\zeta_{nominal}}{S^2}$$

This equation says that the damping factor for a large manipulator is lower than for a small manipulator. Table 3 shows the example parameter set.

Table 3. Example Parameter Set Contrasting a Large Industrial Flexible Robot to Experiment.

	M_{eq}	L_{tot}	C_{tot}	A	ω	ζ
Exper.	0.0912	0.897	128	16	8.076	0.338
"Real"	91.2	8.97	12,800	16	0.8076	0.338

Table 3 shows that a manipulator 10 times as large as the experimental model will need a C_{tot} of approximately 12,800 N-s/m. If one uses two separate dampers in the "realistic" system then both would have coefficients of 6,400 N-s/m. This roughly corresponds to a single damper installed on a large commercial truck hence such dampers exist.

3. CONCLUSIONS

A new configuration for passively damping oscillations in flexible robots was explored. An experimental apparatus demonstrated that one can effectively damp unwanted oscillations using exclusively passive components.

Three areas with potential for further investigation are:

- to apply semi or fully active control using variable damping coefficients as the control input
- to explore the possibility of further weight reduction by using tension-only dampers along with flexible cables allowing a single damper pair to extend the entire beam length
- to explore the possibility of buckling arising from: base actuation, instead of excitation from the tip and center of gravity offset, d1.

REFERENCES

[1] R. Milford and S. Asokanthan, Experimental On-Line Frequency Domain Identification and Adaptive Control of a Flexible Slewing Beam, *Transactions of the ASME*, 118(3), 1996, 58-65.

[2] D. Wang and M. Vidyasagar, Passive Control of a Stiff Flexible Link, *The International Journal of Robotics Research*, 11(6), 1992, 572-578.

[3] T. Alberts, H. Xia, and Y. Chen, Dynamic Analysis to Evaluate Viscoelastic Passive Damping Augmentation for the Space Shuttle Remote Manipulator System, *Transactions of the ASME*, 114(9), 1992, 468-475.

[4] Chih-Min Yao and Wen-Hon Cheng, Joint Space Trajectory Planning for Flexible Manipulators, *Journal of Robotic Systems*, 12(5), 1995, 287-299.

[5] William E. Singhose and Neil C. Singer, Effects of Input Shaping on Two-Dimensional Trajectory Following, *IEEE Transactions on Robotics and Automation*, 12(6), 1996, 881-887.

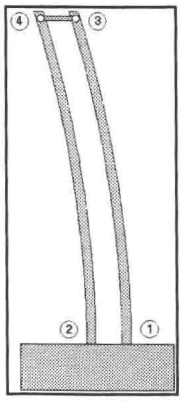

Figure 1 - Parallel Flexible Links.

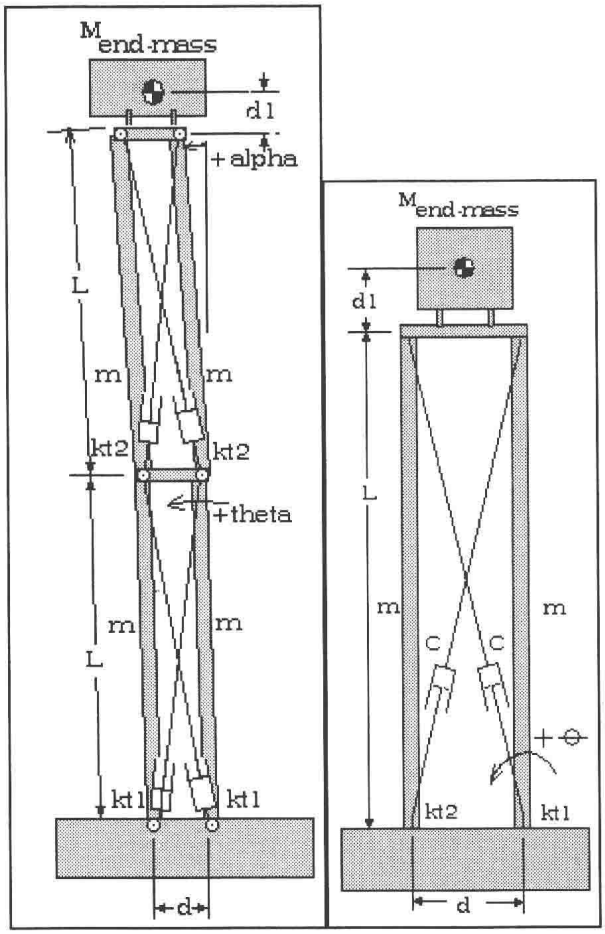

Figure 2 – Multi and single section models.

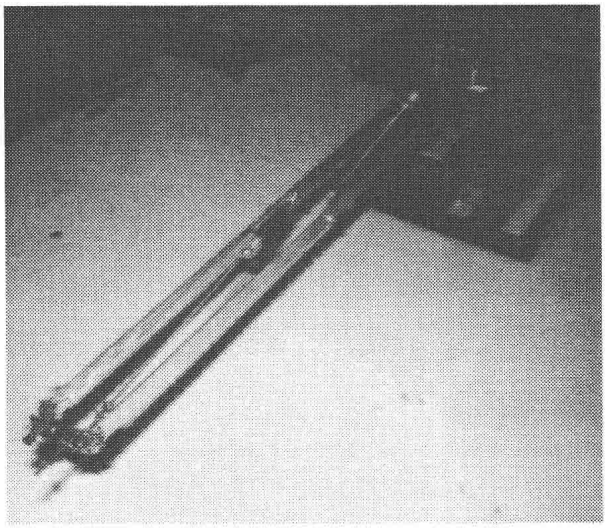

Figure 3 - Experimental device shown with no end mass.

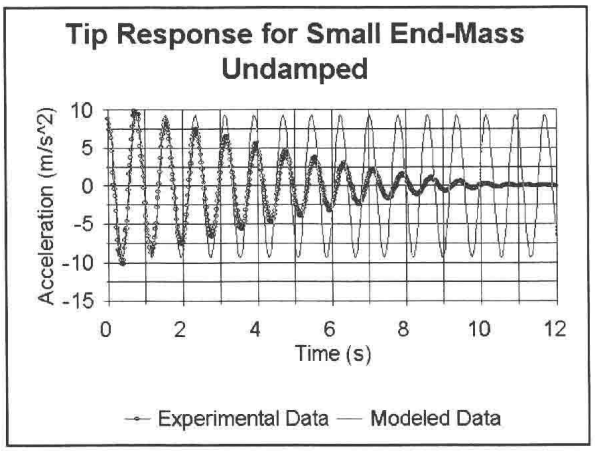

Figure 4 - Typical comparison between measured and computed values.

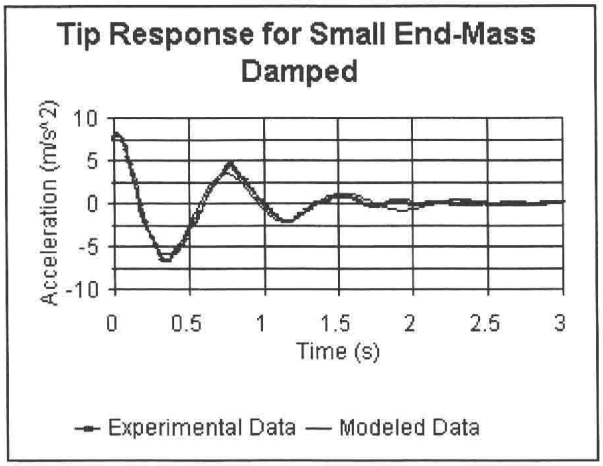

Figure 5 - Typical comparison for the damped case.

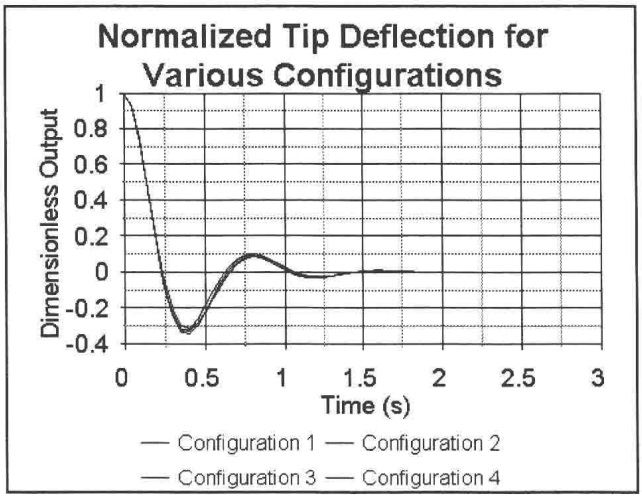

Figure 6 - Tip deflection for several configurations.

Proceedings of the IASTED International Conference
ROBOTICS AND MANUFACTURING
May 21-24, 2001, Cancun, Mexico

DESIGN AND KINEMATIC ANALYSIS OF TERRAIN ADAPTING WHEELED ROBOTIC VEHICLE FOR PLANETARY EXPLORATION

BHARGAV .I. GAJJAR
Teaching and Research Assistant
Mechanical, Materials and Aerospace Engineering Dept.
University of Central Florida
Orlando, Fl 32816 USA
Phone: 407 823 6696
Fax: 407 823 0208
Email: big25455@pegasus.cc.ucf.edu

ROGER W.JOHNSON
Associate Professor
Mechanical, Materials and Aerospace Engineering Dept.
University of Central Florida
Orlando, Fl 32816 USA
Phone: 407 823 2155
Fax: 407 823 0208
Email: rjohnson@pegasus.cc.ucf.edu

Abstract

This paper describes the design and kinematic modeling of unique robotic chassis and suspension of a four-wheeled robotic vehicle. Brief design description is followed by developing wheel Jacobians that relate the chassis velocities with the wheel velocities. The individual matrices for the wheels are combined to form a composite robot solution, which is solved to obtain rover velocities. The rover configuration, which gives the maximum traction, is developed by a dynamic analysis.

1.Introduction

(a) Background

Increased robotic exploration of Mars is essential before the first humans' land on Mars. Surface of planets like Mars is rugged and rocky [19], hence to get stabilized images and smooth body motions it is necessary for the robotic rover to adapt to the terrain suitably. Also it maybe necessary for the robotic vehicle to traverse over rocks. Compared to legged locomotion for robots for planetary exploration, wheeled is presently preferred, because of the complexity of motion and control in the legged robots and low payload capacity. Here an attempt to develop one such unique robotic chassis and suspension of a four wheeled robotic vehicle is done.

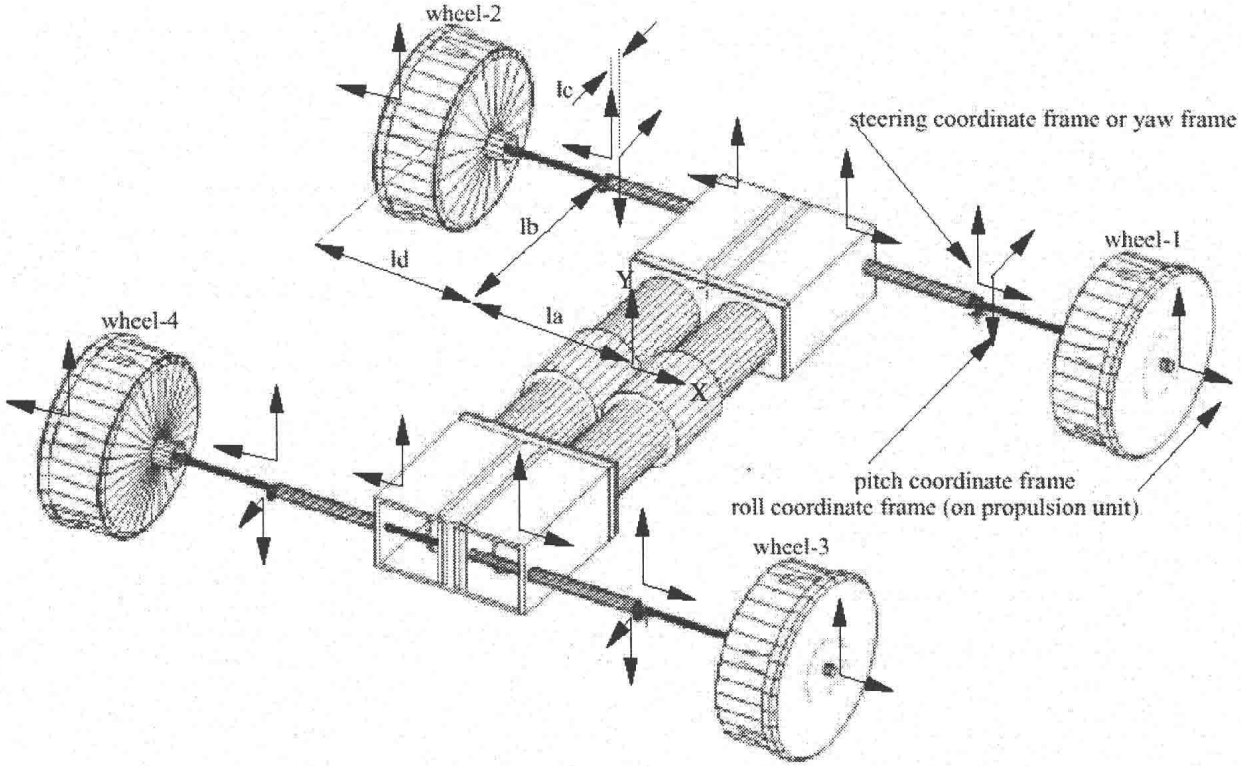

Figure 1 CAD model of robot rover with co- ordinate frames

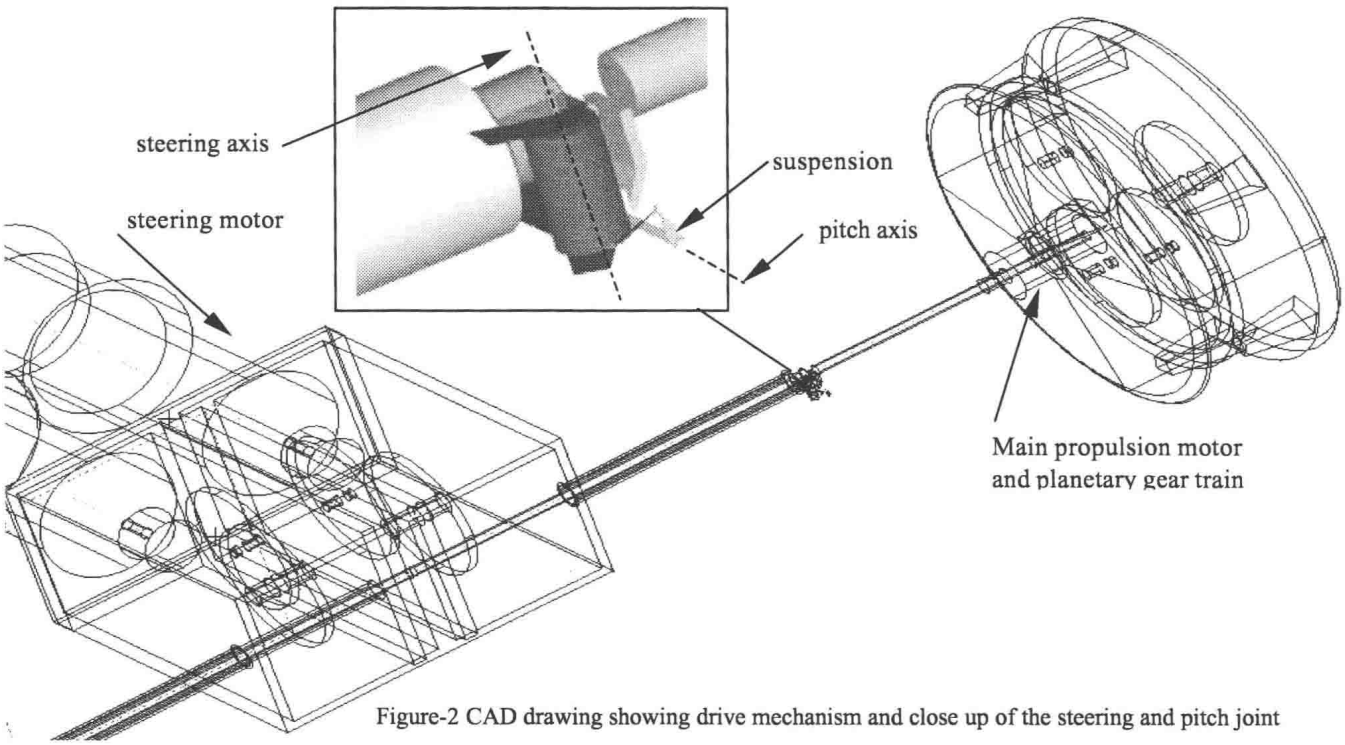

Figure-2 CAD drawing showing drive mechanism and close up of the steering and pitch joint

The NASA Sojourner has demonstrated immense capability of a mobile-wheeled robotic system in remote data acquisition, while traversing over rugged terrain and sending stable pictures. For planetary exploration till date on Moon and Mars, rovers have been preferred over other robots, like legged robots because rovers need to travel over large distances over a given time period and analyze and manipulate soil and rock samples [1].

(b) Objective

While terrain adaptable robotic rovers like Nomad [2] use a unique mechanism like expanding chassis to stabilize the sensing platform, rovers like Sojourner use the rocker-bogie mechanism to stabilize the sensing and communications platform [3]. The rocker bogie configuration is planar mechanism and has been modeled thus [4], [5]. Planar rocker-bogie has 2 DOFs associated with it, the pitch and the yaw, where in the yaw affects the steering. In this paper a robotic-wheeled chassis is developed which can effectively adapt to any type of rocky terrain in 3 D and has 3 degrees of freedom, also a suspension which effectively improves ground traction This paper describes the design of the robot chassis, and kinematic modeling followed by a dynamic analysis .

2.Mechanical Design of the 3-DOF wheeled robotic chassis

Here an entirely new system of suspension has been developed to connect the wheel of the rover to the main platform, which carries the solar array, camera and science experiment package. There are 2 independent shafts, which are interconnected by a motor. One shaft is for the pitch and the other for the yaw and steering simultaneously. The propulsion or the drive motor is attached to the pitchshaft end, and couples to the wheel as shown in figure 2. In this way we have a 4-wheel independent steering as well as 4 wheel independent drive for increased power over rugged terrain. The steering motor driving the yaw arm is mounted on rover platform and drives the yaw axis along with steering through a worm and worm wheel arrangement. The spring on the yaw end of the shaft provides passive suspension. The steering motor not only controls the steering when required but can also provide active vibration control of the yaw movement, during normal motion over obstacles. Also with simple future modifications the wheels can be comfortably collapsed and folded and stowed in the payload of a spacecraft given the initial design volumetric constraints.

Since the obstacles that the rover is expected to encounter and surmount are fairly large - on the order of the size of the wheels - the loss of capability to negotiate an obstacle is not acceptable. The suspension in this system is expected to create a normal force significant to create traction, because of the fact that the wheel always remains perpendicular to the surface it tries to negotiate, and in turn imparts a normal force and causes the treads to remain in contact all the time for traction. This can be a significant advantage over other mechanisms. In equalizing the forces at the 4 wheels of rover, the 3 DOF system compensates for the adjustment to be done by software or hardware means for the communication system. Averaging motion is affected significantly by adjusting the length of the linkages or as in this case changing the spacing between the wheels by the mechanism employed. Because this can imply a change in wheelbase as well, these sizes can also affect other aspects of the rover's terrainability [6]. This

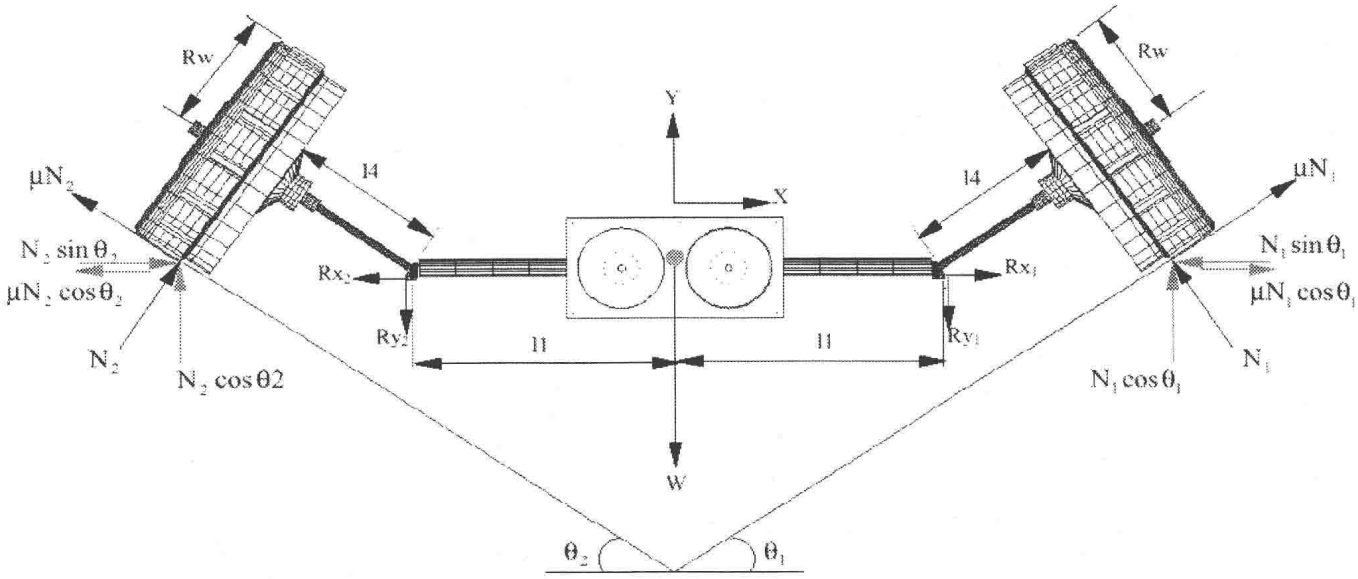

Figure-3 Forces on the rover

can also be achieved in this robotic chassis, and averaging motion of the sensing platform is expected to be minimum.

The prototype has currently the following overall dimensions: 48 cm wide, 64 cm long and 32 cm high, with 4 wheels each of diameter 13 cm. These dimensions are taken according to the Mars Rover prototype Rocky 7[7] experiments.

Similar effects occur for pitch and roll.

Averaging movement of the rover is simply the vertical displacement of the geometric center of the body and is the average of the displacements of the wheels. With the communications requirements playing a major part in the design, this averaging, is particularly important.

Averaging is minimized in this robot rover by the folding of the wheels and adjusting to the terrain.

3.Forward Kinematic Analysis

The following assumptions are made for kinematic modeling of this robot:

(a) A single contact point of each of the four wheels with the terrain.

(b) Pure rolling motion only at each of the four wheels, which means that the component of the velocity at the contact point of each wheel with ground in the plane of the wheel is zero.

(c) There is no wheel slip, which means that the component of the velocity at the contact point of each wheel with ground orthogonal to the plane of the wheel is zero.

(d) Each of the 4 wheels is a conventional steered wheel.

(e) The conventional wheel has 2 DOF, which allows it to move along the direction of rolling of the wheel and also turn and steer about the point of contact.

(f) All the links of the robot rover are absolutely rigid.

(g) All the wheels are having a steering capability.

(h) All steering axes are perpendicular to the surface.

Only 2 out of 3 DOF of the robot are actuated, the steering and the roll. The pitch is passive and depends on the terrain. This is an inherent characteristic of all wheeled mobile robots.

The coordinate frames are assigned on the rover chassis and the wheels using the convention in [8] as shown in figure-1 and the Jacobian matrices below. Thus the wheel Jacobians relate individual wheel velocities to the rover velocities:

4 Composite robot equation formulation

Getting the wheel Jacobians relating each of the 4 wheel

$$\begin{bmatrix} V_{Rx} \\ V_{Ry} \\ \omega_R \end{bmatrix} = \begin{bmatrix} 0 & l_b & -l_b \\ R_w & l_a + l_d & l_a \\ 0 & 1 & -1 \end{bmatrix} \begin{bmatrix} \omega_{w1x} \\ \omega_{w1y} \\ \omega_{w1z} \end{bmatrix} \qquad \begin{bmatrix} V_{Rx} \\ V_{Ry} \\ \omega_R \end{bmatrix} = \begin{bmatrix} 0 & l_b & -l_b \\ R_w & l_a - l_d & -l_a \\ 0 & 1 & -1 \end{bmatrix} \begin{bmatrix} \omega_{w2x} \\ \omega_{w2y} \\ \omega_{w2z} \end{bmatrix}$$

$$\dot{p}_1 = J_1 \cdot \dot{q}_1 \qquad \dot{p}_2 = J_2 \cdot \dot{q}_2$$

$$\begin{bmatrix} V_{Rx} \\ V_{Ry} \\ \omega_R \end{bmatrix} = \begin{bmatrix} 0 & l_b & -l_b \\ R_w & l_a - l_d & -l_a \\ 0 & 1 & -1 \end{bmatrix} \begin{bmatrix} \omega_{w3x} \\ \omega_{w3y} \\ \omega_{w3z} \end{bmatrix} \qquad \begin{bmatrix} V_{Rx} \\ V_{Ry} \\ \omega_R \end{bmatrix} = \begin{bmatrix} 0 & -l_b & l_b \\ R_w & l_a - l_d & -l_a \\ 0 & 1 & -1 \end{bmatrix} \begin{bmatrix} \omega_{w4x} \\ \omega_{w4y} \\ \omega_{w4z} \end{bmatrix}$$

$$\dot{p}_3 = J_2 \cdot \dot{q}_2 \qquad \dot{p}_4 = J_4 \cdot \dot{q}_4$$

velocities to the rover velocity, it is now possible to combine these equations into a composite equation and find the solution of it. The composite equation has the following form:

$$\begin{bmatrix} I_1 \\ I_2 \\ I_3 \\ \vdots \\ I_n \end{bmatrix} \dot{P} = \begin{bmatrix} J_1 & 0 \cdots & 0 \\ 0 & J_2 & \ddots \\ \vdots & \ddots & \ddots & 0 \\ 0 & \cdots & 0 & J_N \end{bmatrix} \begin{bmatrix} \dot{q}_1 \\ \dot{q}_2 \\ \vdots \\ \dot{q}_N \end{bmatrix}$$

$$A\dot{p} = B\dot{q}$$

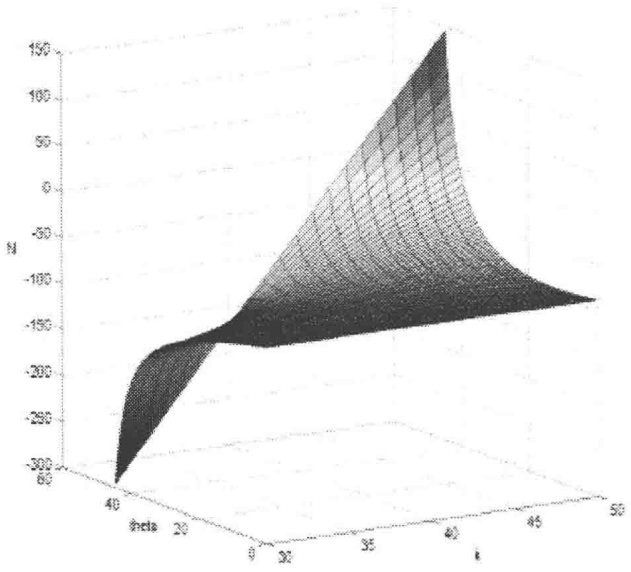

Figure-4 Plot of Normal force (N) vs. Theta (degrees) vs. Stiffness (N/m)

Rover velocities are given by [8] using [20]

$$\dot{p}=(A^TA)^{-1}A^TB\dot{q}$$

$$\begin{bmatrix}1&0&0\\0&1&0\\0&0&1\\1&0&0\\0&1&0\\0&0&1\\1&0&0\\0&1&0\\0&0&1\\1&0&0\\0&1&0\\0&0&1\end{bmatrix}\begin{bmatrix}V_{Rx}\\V_{Ry}\\\omega_R\end{bmatrix}=\begin{bmatrix}0&l_b&-l_b&0&0&0&0&0&0&0&0&0\\R_w&l_a+l_d&l_a&0&0&0&0&0&0&0&0&0\\0&1&-1&0&0&0&0&0&0&0&0&0\\0&0&0&0&l_b&-l_b&0&0&0&0&0&0\\0&0&0&R_w&-l_d+l_a&-l_a&0&0&0&0&0&0\\0&0&0&0&1&-1&0&0&0&0&0&0\\0&0&0&0&0&0&0&-l_b&l_b&0&0&0\\0&0&0&0&0&0&R_w&-(l_a+l_d)&l_a&0&0&0\\0&0&0&0&0&0&0&1&-1&0&0&0\\0&0&0&0&0&0&0&0&0&0&-l_b&l_b\\0&0&0&0&0&0&0&0&0&R_w&-l_d+l_a&-l_a\\0&0&0&0&0&0&0&0&0&0&1&-1\end{bmatrix}\begin{bmatrix}\omega_{1x}\\\omega_{1y}\\\omega_{1z}\\\omega_{2x}\\\omega_{2y}\\\omega_{2z}\\\omega_{3x}\\\omega_{3y}\\\omega_{3z}\\\omega_{4x}\\\omega_{4y}\\\omega_{4z}\end{bmatrix}$$

Here x direction angular velocity on the axle and the z direction angular velocity on the steering shaft are measured by shaft integral digital encoders. The angular velocity at the axle end along z direction is assumed zero because of pure rolling conditions only.

The rover chassis velocities knowing the wheel velocities are as below:

$$V_{Rx}=0.25\cdot l_b\cdot\omega_{1y}-0.25\cdot l_b\cdot\omega_{1z}+0.25\cdot l_b\cdot\omega_{2y}-0.25\cdot l_b\cdot\omega_{2z}$$
$$+0.25\cdot l_b\cdot\omega_{3y}-0.25\cdot l_b\cdot\omega_{3z}+0.25\cdot l_b\cdot\omega_{4y}-0.25\cdot l_b\cdot\omega_{4z}$$
$$V_{Ry}=0.25\cdot R_w\cdot\omega_{1x}+0.25\cdot(l_a+l_d)\cdot\omega_{1y}+0.25\cdot l_a\omega_{1z}+0.25\cdot R_w\cdot\omega_{2x}$$
$$+0.25\cdot(l_a-l_d)\cdot\omega_{2y}-0.25\cdot l_a\omega_{2z}+0.25\cdot R_w\cdot\omega_{3x}+0.25\cdot(l_a-l_d)\cdot\omega_{3y}$$
$$-0.25\cdot l_a\omega_{3z}+0.25\cdot R_w\cdot\omega_{4x}+0.25\cdot(l_a-l_d)\cdot\omega_{4y}-0.25\cdot l_a\cdot\omega_{4z}$$
$$\omega_R=0.25\cdot(\omega_{1y}-\omega_{1z}+\omega_{2y}-\omega_{2z}+\omega_{3y}-\omega_{3z}+\omega_{4y}-\omega_{4z})$$

5.Planar dynamic analysis to find optimum chassis dimensions

Adequate traction is key to success of a Planetary rover. The rover linkage with wheel is analyzed in a x-y plane to compute the traction force exerted by the wheel on an inclined obstacle as shown in figure 3. In a previous

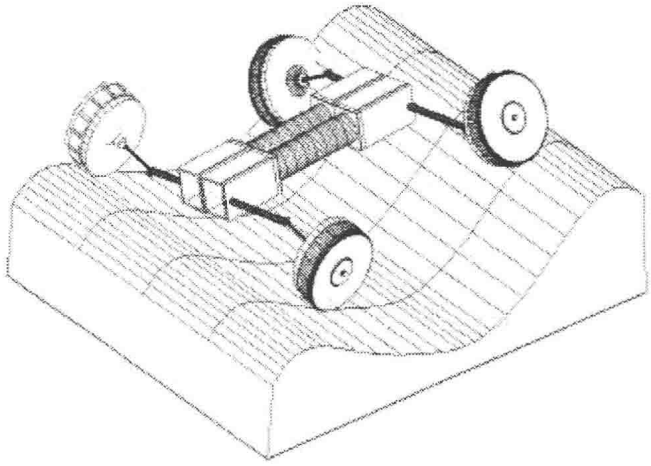

Figure-5 Robot in motion over uneven terrain

paper planar static analysis has been carried out for the Mars Rocker Bogie [4]. Here a dynamic analysis is attempted. The equilibrium equations are obtained by summing forces in the x and the y directions and taking moments about the hinge points 1 and 2 for the entire vehicle as viewed from the front. The inclined plane angle is varied by 1 degrees from 0 to 45 degrees. Any further increase in the slope angle results in the wheel crashing on the sensing platform in this configuration. For simplified analysis it can be assumed that the slope angles are equal on either side. The traction force, which is perpendicular to the normal to the ground, is evaluated in each case of varying the length parameters of the rover linkage with the wheel and the wheel radius. The spring constant is assumed along with coefficient of friction for the tire material. It is also assumed that the slope angle does not practically vary with the height of the slope. The no wheel slip condition and a single point of contact of the wheel with the ground also hold true in this case. A computer program has been developed [20] to successively change these variables and plot the slope angle with the traction force.

6.Conclusions

A kinematic model of the rover has been prepared, which enables to compute the chassis speeds relative to the rate of change of wheel articulation angle. Since the wheel articulation angle in the x direction can be sensed, by shaft mounted encoder, using rolling and zero slip assumptions it's possible to know the rover chassis velocity with respect to the ground. This data can be used as a feedback, to adjust the angular position of the wheel linkage over a terrain to stabilize the sensing platform of the rover. The feedback can be given to a motion sensor mounted on the sensor platform like an inertial rate gyro. The dynamic analysis provides a configuration, which gives highest traction over the tallest obstacle. It is also observed that this design must be optimized to fit the payload bay of the delivering spacecraft along with its terrain adaptive performance. The traction is related to the normal force by

the coefficient of friction. In this design the terrain adaptable mechanism is so developed as to impart a greater normal force and thus to increase the ground traction. It is observed from the plots, in figure-4 that for a given spring coefficient, as the obstacle angle increases the traction force increases due to the inherent nature of the design to deflect spring more as the degree of obstacle negotiation increases. Also it is seen that each wheel imparts a normal force which is dependent on how steep a terrain it is negotiating.

7.References

[1] Klaus, S., Jungius, C., "Mobile robots for planetary exploration", IFAC intelligent autonomous vehicles, Espoo Finland, 12-14 June 1995

[2] Wettergreen, D., Bapna, D., Maimone, M., Thomas, H., "Developing Nomad for robotic exploration of Atacama desert", *Robotics and Autonomous Systems*, Vol. 26, No. 2-3, Feb 1999,

[3] NASA Intelligent machines group: http://img.arc.nasa.gov/

[4] Linderman, R., Eisen, H., "Mobility Analysis, Simulation and scale model testing for design of wheeled planetary rovers", In mission technologies and design of mobile planetary vehicle 531-37 Toulouse France, Sept 1992.

[5] Harcot, H., Dubowsky, S., Philippe, B., "Analysis and Simulation of a Rocker Bogie Exploration Rover" Mechanical engineering at MIT (publication).

[6] The Lunar Rover Initiative website at Robotics institute at Carnegie Mellon http://www.frc.ri.cmu.edu/projects/lri/Luna/report/loco.html#HDR2).

[7] Tarokh, M., Mc Dermot, G., Hayati, S., Hung, J., "Kinematic Modeling of High Mobility Mars Rover", Proceedings of IEEE International conference on Robotics and Automation, Detroit Michigan, May1999.

[8] Muir, P., Neumann, C.P., "Kinematic Modeling of wheeled mobile robots", Journal of Robotic Systems, Vol.4, No.2, pp.281-340, 1987.

[9] Rivin, E., *Mechanical Design of Robots* (McGraw-Hill, Inc., 1988)

[10] Tsai, L., *Robot Analysis* (New York: John Wiley and Sons Inc., 1999)

[10] Craig, J., *Introduction to Robotics Mechanics and Control* (Reading, Massachusetts Addison-Wesley Publishing Company, Inc., 1955)

[11] Kang, D., Anderson, J., Debitetto, P., "Draper Unmanned Vehicle Systems", IFAC International Autonomous Vehicles, Madrid, Spain, 1988.

[12] Hayati, S., "Robotic Planetary Surface Exploration", International Autonomous Vehicle Systems", Madrid, Spain, 1988.

[13] Dubowsky, S., Cole, J., Rutman, N. and Sunada, C. "Mobile Autonomous Robotics Systems for Unstructured Environments – with Application to the USS Constitution." *Proceedings of the NSF Design and Manufacturing Grantees Conference*, San Diego, CA, January 4-6, 1995. Invited.

[14] Farritor, S., Hacot, H., and Dubowsky, S. "Physics-Based Planning for Planetary Exploration." 1998 IEEE International Conference on Robotics and Automation, Leuven, Belgium, May 1998. Vol.1, 1998, pp. 278 –283

[15] Huntsberger, T.L., Baumgartner, E. T., Aghazarian, H., Cheng, Y., Schenker, P. S., Leger, P.C., Iagnemma, K.D., and Dubowsky, S., "Sensor-Fused Autonomous Guidance of a Mobile Robot and Applications to Mars Sample Return Operations", *SPIE's International Symposium on Intelligent Systems and Advanced Manufacturing*, September 1999

[16] Iagnemma, K., and Dubowsky, S., "Vehicle Wheel-Ground Contact Angle Estimation: With Application to Mobile Robot Traction Control", *Proceedings 7th International Symposium On Advances in Robot Kinematics, Piran-Portoroz, Slovenia,* June 2000

[17] Joseph, J., Flynn, A., *Mobile Robots: Inspiration to Implementation,* (Wellesley, MA, A K Peters, 1993

[18] Shetty, D., Kolk, R., *Mechatronics System Design* (Boston: PWS Publishers Inc, 1997)

[19] Hayati, S., Volpe, R., Backes, P., Balaram, J., Welch, R., Ivlev, R., Tharp, G., Peters, S., Ohm, T., Petras, R., Laubach, S., "The Rocky 7 Rover: A Mars Sciencecraft Prototype", Proceedings of the 1997 IEEE International Conference on Robotics and Automation, Albuquerque, New Mexico-April 1997

[20] MATLAB Version 5.3.0.14912a (R11) on PCWIN, MATLAB Toolbox Version 5.3 (R11), MATLAB Symbolic Toolbox Version 5.3 (R11)

Proceedings of the IASTED International Conference
ROBOTICS AND MANUFACTURING
May 21-24, 2001, Cancun, Mexico

CONFINED MORPHOLOGICAL CHOICE OF PLANAR KINEMATIC MECHANISMS IN ROBOTICS

Peter MITROUCHEV

Integrated Design Center, "Sols, Solids, Structures - 3S" Laboratory, UMR 5521, Domaine Universitaire, B.P. n° 53, 38041 GRENOBLE Cedex 9, France, phone (33) 4 76 82 51 25, Fax. (33) 4 76 82 70 43, E-mail: Peter.Mitrouchev@hmg.inpg.fr

ABSTRACT

In this paper a morphological confined choice for kinematic mechanisms in robotics is presented. It is based on symmetries of structures. The number of possible configurations is confined by eliminating the symmetrical ones. Different cases of symmetries have been studied. An expression for the calculation of the number of frames and end-effectors is presented. It enables the reduction of the number of structures by avoiding those that are isomorphic. Following this, examples for applications for various kinematic structures are presented, enabling the field of research to be restricted to the possible solutions.

KEY WORDS: morphology, planar mechanisms, robotics.

1. Introduction

The choice of a kinematic mechanism applied in robotics is conditioned by the number of degrees of freedom of the task to be carried out by the robot. The task itself imposes a kinematic chain compatible with its number of degrees of freedom. The kinematic chain thus imposed will be compatible with the task if it possesses a number and type of links and joints as those defined by the mobility and connection laws of Mechanism and Machine Theory (MMT). MMT supplies the list of possible mechanisms. As there may be a large number of these mechanisms, it is usually difficult to make a choice amongst the available structures in the initial design phase of the robot chain. In fact taking into account the symmetries it can be noticed that there are a significant number of isomorphic structures as far as the position of the frame and of the end-effector of the robot.

MMT contributed greatly to planar and spatial mechanism synthesis with different degrees of freedom [1, 2, 3, 4, 5, 6, 7]. Some of the current industrial robots with planar chains have a structure created by the kinematic graphs of MMT [1, 8, 9].

The morphological (topological) synthesis of kinematic chains has, for a long time, been the subject of many papers. There exist different methods for the kinematic synthesis of planar chains with simple revolute joints, with different degrees of mobility and different numbers of links and joints. These methods which enabled the lists of chains, called A_i lists, to be obtained are: intuition and inspection [8], graph theory [10, 11]. Others consist of transformation of binary chains [2, 4, 12, 13] the concept of Assur groups [9, 14, 15], or Franke's notation [16, 17]. New methods based on genetic algorithms or neuronal networks are also used [18, 19]. These A_i lists are subdivided into many sub-lists B_i taking into account the position of the frame and of the end-effector of the robot.

The problem is how to choose amongst the possible structures provided by MMT as far as the position of the frame and the end-effector. The aim of this paper is to present a new method enabling the reduction of the number of kinematic structures provided by the MMT which are suitable for robotics applications. It is based on the exploitation of symmetries of the mechanisms. The sub-lists B_i are then studied in order to extract the minimum number of possible structures for the initial design of kinematic chains of industrial robots, the two criteria being the position of the frame and of the end-effector of the robot.

2. Notations and restrictions

MMT proposes various ways of representing kinematic structures. The most common, the *kinematic graph*, consists in conserving a shape for the links in order to better appraise the topology of the structure. Nevertheless this presentation is difficult to manage. Any kinematic structure may by transformed into Crossley's *inverse graph* [8, 20] replacing every link (binary, ternary...) by a point. The joints themselves are represented by a line linking the points concerned. The kinematic graph expresses geometrical dimensions. Obviously the inverse graph does not.

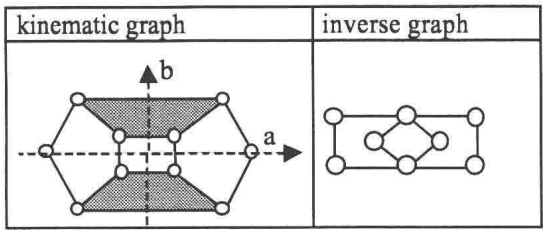

Fig. 1. Representation of a structure by Crossley's inverse graph

The Manipulation System (MS) of a robot is a mechanism used to position and to orient an object or an end-effector in space. It is noted at this stage that the structure presented by one or other method only presents the main structure of the robot. A robot being a complex mechanical system characterized by a very important interaction between its links, we define its architecture by [21]:

- the *main structure*, which generates the main motion of the robot and upon which, stands the rest of the MS,
- the *regional structure*, consisting of the arm and the forearm of the robot (mechanical arm),
- the *local structure* usually consisting of three axes concurrent at one point, and representing the wrist of the robot.

Let us consider a mechanism with N links of any type, joined to each other by C_5 simple revolute joints with one degree of freedom. In this paper only mechanisms having main planar structures with simple revolute joints usually applied in robotic design will be studied.

3. Mechanism design

MMT, being a part of the technological sciences is at the base of mechanism design in robotics. The question now is: amongst the available kinematic structures supplied by MMT, how many of these are suitable for application in kinematic chain design in robotics? In order to reply to the above question it is interesting to answer the following ones: why and how?

3.1 Why?

Obviously it is not possible to dimension a mechanism without being familiar with its topology. The topological choice is normally made before the dimensioning phase. It is this stage that presents the most difficult problem in mechanism synthesis. It is currently impossible to place the dimensioning equations on the same level as the choice of topology, because this choice is not governed by equations i.e. assigning design variables for this or that topology, except for: degree of mobility M, number of links N and number of joints C_5 (e.g. M=2, N=7 and C_5=8).

3.2 How?

The problem is deciding which structures may be removed from the A_i list, without restricting the choice of available structures. The B_i list, issue from an A_i list, has some structures listed twice, taking into account the position of the frame and of the end-effector.

Let us consider an A_i list of P topologies Topo i extracted from a complete list of mechanisms with respect to some parameters (e.g. mechanisms with one degree of mobility M=1, eight links N=8 and ten joints C_5=10). Firstly from this list P, B_i sub-lists are extracted with respect to criterion 1 "fixing a frame" or "frame choice". Then each topology Topo i gives several possibilities for attaching an end-effector (pincers, paint gun, welding electrode, ...[22]). This is the second criterion "fixing an end-effector" or "end-effector choice" with regard to the choice of the frame used in the elaboration of the confined B_i lists. For example, the B_i list of fig. 2 contains N(N-1)=7.6 = 42 possible solutions but it is noted that some of them appear twice: solutions 1 and 6, 2 and 5, 4 and 3 for the first possibility to fix a frame. For the other possibilities it is reasonable to suppose that there will be other dual (isomorphic) solutions. Therefore the following two observations can be made:

- The problem of fixing a frame and an end-effector is a symmetric one in the sense that it is same thing to fix a frame then to see the possibilities for fixing an end-effector to the remaining links and vice versa. In the proposed example, the frame has been fixed, then the possibilities for fixing an end-effector were investigated.
- If solutions appear twice, it is because of symmetry.

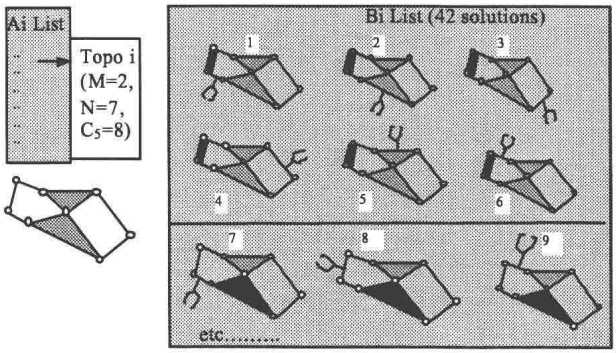

key: black element - frame, ⊣ end -effector

Fig. 2. Elaboration of the B_i list

4. Proposed method

4.1 Notations :

- N number of the links,
- Fc (frame choice) the number of different possibilities to fix a frame onto a chain,